PHYSICAL REVIEW E **77**, 030602(R) (2008)

Scale-invariant competitive growth of side branches in a dendritic crystal

Kazuki Kishinawa, Haruo Honjo, and Hidetsugu Sakaguchi
Department of Applied Science for Electronics and Materials, Interdisciplinary Graduate School of Engineering Sciences, Kyushu University, 6-1 Kasuga Koen, Kasuga, Fukuoka 816-8580, Japan

(Received 21 December 2007; revised manuscript received 28 February 2008; published 28 March 2008)

We experimentally investigated statistical properties of side branches of quasi-two-dimensional NH_4Cl dendritic crystals. The height distributions of the side branches and their number density exhibit scale-invariant power laws. The results are in good agreement with the results of numerical simulations and theories of diffusion-limited needle growth. Our scaling exponents are independent of supersaturation and the statistical properties are universal in dendrites.

DOI: 10.1103/PhysRevE.77.030602 PACS number(s): 68.70.+w, 61.43.Hv, 81.10.Dn, 05.45.Df

I. INTRODUCTION

Pattern formation in a diffusion field has been studied as a typical nonequilibrium phenomenon, e.g., diffusion-limited aggregation (DLA) [1], dense-branching morphology [2], and dendrites [3,4]. We can also observe these patterns in crystal growth [3,4] and electrochemical deposition [5]. The patterns have innumerable branches that are generated by the Mullins-Sekerka instability [6], and the branches compete against each other. This growth competition among the branches results in various complicated structures, and the statistical characteristics of the patterns depend on the degrees of nonequilibrium and anisotropy [7].

Dendrites of xenon, succinonitrile, and NH_4Cl can be observed experimentally. The tip velocity [3,8] and the shape near the tip region [9,10] have been intensively studied experimentally and theoretically as a typical nonlinear problem. On the other hand, the global structure that results from the competitive growth of the side branches has been characterized by various parameters. The angle of the envelope increases with the distance from the stem tip up to 45° [4,11–13], and the internal structure that consists of branches of various sizes is considerably complicated. The projected pattern of a dendrite has been characterized by fractal dimensions [14–17]. Moreover, it has been revealed that the other geometric parameters, such as mean shape [18,19], contour length, and projection area (surface area and volume), as a function of the distance from the tip show scaling laws [11,14,16,17,20,21].

In a previous paper, we have studied the competitive growth of side branches in a dendritic pattern [22] using a coupled map lattice (CML) model [23]. We have shown that the growth velocities of shorter branches depend on the geometrical structure of competing higher branches, and this dependence follows an exponential decay law for the growth velocity of the shorter branches. The results are qualitatively consistent with the experimental results of dendritic crystal growth of NH_4Br [24]. The CML model shows that the height distributions of the branches exhibit a power law. The result is in good agreement with the results of a Laplacian needle growth model, which has been proposed by Rossi [25,26] and Meakin [27] as a DLA model without both tip-splitting and branching. In this model, needles grow only in the perpendicular direction to a line seed. This model exhibits a feature in which needles whose growth was stopped by other branches invariably obey the following scaling laws of their height distribution $N(h)$ and density profile $\rho(h)$ at height h from the seed:

$$N(h) \propto h^{-\alpha}, \tag{1}$$

$$\rho(h) \propto h^{-\beta}. \tag{2}$$

In a large-scale simulation, the scaling exponents α and β obey the relation $\alpha=\beta+1$. Laplacian needle growth has been the most commonly studied mechanism for scale-invariant growth [28,29]. The results of these studies show fractality of the competitive growth and the structure of the branches and Laplacian needles.

On the other hand, it has been predicted that diffusion-limited growth, such as in polymer brushes [30] and dendritic crystals in directional solidification [31], would generate an additional structure according to the scaling laws. However, these predictions have never been confirmed experimentally.

We conducted experiments to investigate the height distributions and number density profiles of side branches in NH_4Cl dendritic crystals in various supersaturated solutions. The distributions and profiles exhibit scale-invariant power laws, and our results agree with both the results of numerical simulations and theories of diffusion-limited needle growth.

II. EXPERIMENT

We performed experiments in a Hele-Shaw cell that has a narrow space within two slide glasses; the thickness d of the spacer is 100 μm (Fig. 1 [32]). An NH_4Cl aqueous solution saturated at approximately 40 °C is enclosed in the cell. Crystal growth is observed once the cell temperature is low-

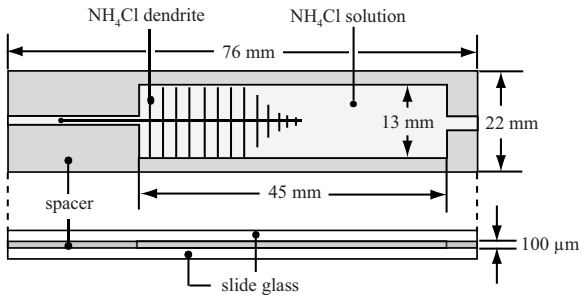

FIG. 1. Cell structure.

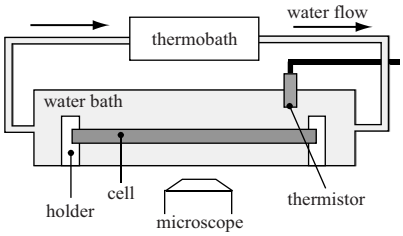

FIG. 2. Experimental setup.

ered below the saturation temperature. The cell temperature is controlled by water flow of the thermobath with an accuracy of ± 0.003 °C, which is calculated from the measured resistance of the thermistor in the water bath (see Fig. 2). Nucleation occurs at the narrow path in the cell, and the dendrite grows along it into the wide region for observation. An NH_4Cl dendrite has four-fold symmetry, and the tip growth direction is ⟨100⟩. The spatial dimension of our system is conditioned by the relation between the diffusion length $l_D=2D/v$ and d, where D is the diffusion constant of the NH_4Cl solution (2.6×10^3 $\mu m^2/sec$ [33]) and v is the tip velocity of the stem. In our experiment, v is approximately between 34 and 72 $\mu m/sec$; therefore, l_D is 72 $\mu m \leqslant l_D \leqslant 153$ μm. Because the velocity of the branches is much less than that of the stem, l_D for the branch is much greater than d; therefore, the branches form a quasi-two-dimensional system. The growing dendrite is observed using an inverted microscope and a CCD camera whose image resolution is 640×480 pixels. The images are recorded at 30 fps with 8-bit intensity and are analyzed using a personal computer. After subtraction of the background image, the intensity profile of the tip along the stem, which has a sigmoid curve, is measured. We select the point of inflection of the curve as the threshold of binarization of the images. The method has an accuracy of approximately ± 1 pixel.

III. RESULTS AND DISCUSSION

Figures 3(a) and 3(b) shows time sequences of typical growing dendrites (from top to bottom), which are observed with different microscopic magnifications corresponding to resolutions of 0.55 and 5.49 $\mu m/pixel$, respectively. The tip velocity V is 34 ± 1 $\mu m/sec$. Many branches are successively generated at the region near the growing tip. The growth of the shorter branches is stopped by a few neighboring higher branches due to a screening effect, and the growth of some higher branches is similarly stopped by even higher branches. This competitive growth dynamics occurs successively over an expansion of the competitive radius, and the global branching structure consists of nests of branches [Fig. 3(b)].

In the images, the x axis is defined as a line along a stem, and it passes through the tip of the stem. The y axis is defined as a line perpendicular to the x axis, and is in the growth direction of the branches. The height h of each branch is measured from the x axis just before the occurrence of dendritic coarsening [4]. After the branches stop growing, they begin to shrink due to the coarsening effect. In Fig. 5, the branches except for the lapped ones from the images stop

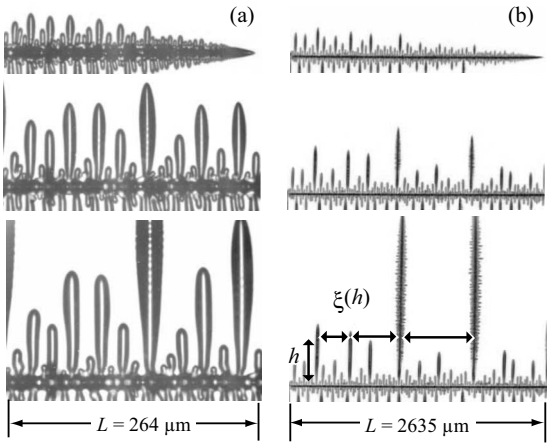

FIG. 3. Time sequences of a typical dendrite ($V=34$ $\mu m/sec$) for different microscope magnifications. From top to bottom, (a) the images are captured every 14 sec and $L=264$ μm, and (b) the images are captured every 60 sec and $L=2635$ μm.

growing, and are measured. In this case, the dendritic coarsening effect is ignored because of low resolution of the image. We define the number density profile $\rho(h)$ as the reciprocal of the interval average $\langle\xi(h)\rangle$, which is expressed as $\langle\xi(h)\rangle=\int_0^\infty \xi(h)P(\xi)d\xi$. Here, $\xi(h)$ is the interval of branches, as indicated in Fig. 3(b), and $P(\xi)$ is the normalized number distribution of $\xi(h)$. The standard deviation of $\langle\xi(h)\rangle$ is large (approximately 30%) because of the large variance of $P(\xi)$. We compiled statistics on the height h and interval $\xi(h)$ from 28 different regions with width $L=264$ μm, as shown in Fig. 3(a) and 16 different regions with $L=2635$ μm, as shown in Figs. 3(b) and 5.

Figure 4(a) shows the height distributions $N(h)$ of the branches shown in Figs. 3(a) and 3(b), which exhibit a scaling law such as Eq. (1). The data of higher branches are more dispersed than that of shorter branches, because the samples for the higher branches are fewer than that of the shorter ones. The values of the exponent α are obtained by linear regression, and their errors are standard errors of the regression coefficients. Figure 4(b) shows the number density profiles $\rho(h)$, which overlap well and exhibit a scaling law such as Eq. (2). The profiles are much less noisy than the height distributions due to averaging. The values of the exponent β are obtained by linear regression using a weight of the standard deviation of the $\rho(h)$ in the same regions as the fitted regions of the distributions. We show the values of α and β of each L in Table I. In the fitted regions, the error bars of h are within the symbols, and the scattering of $N(h)$ is sufficiently larger than the symbols [see Fig. 4(a)]. The error of h (less than 10%) is not significant relative to the statistical errors of $\rho(h)$ (approximately 30%). Therefore, we ignore the error in h.

Figure 5(a)–5(c) show three different dendrites at higher supersaturations than the dendrites shown in Fig. 3, and $V=49$, 57, and 72 $\mu m/sec$ with an accuracy of approximately ± 1 $\mu m/sec$, respectively. As the dendrite growth speed increases, its structure becomes denser with more side branches growing on the branches.

Figures 6 and 7 show $N(h)$ and $\rho(h)$ of the branches shown in Fig. 5(a)–5(c), which also exhibit power laws.

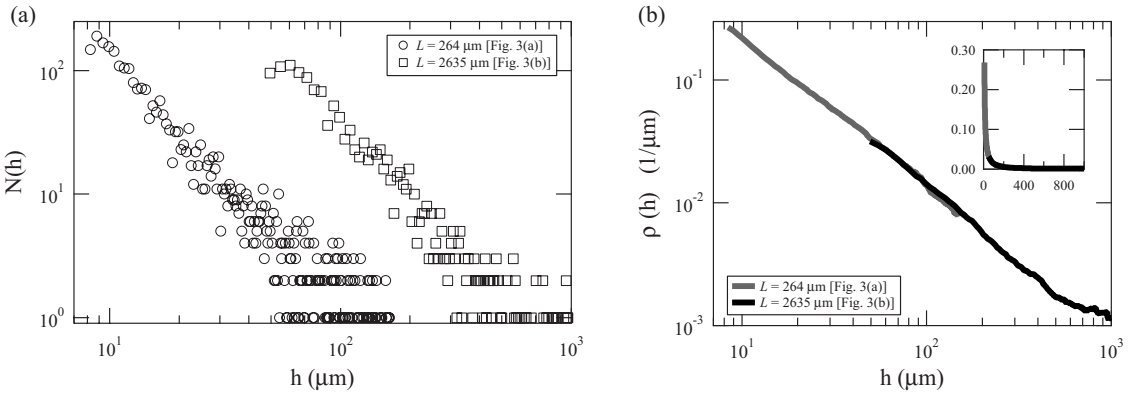

FIG. 4. (a) Height distributions and (b) number density profiles of the branches of dendrites with $V=34$ μm/sec and $L=264$ and 2635 μm shown in Figs. 3(a) and 3(b).

These profiles clearly have linear and nonlinear regions. The fittings are performed by the same methods as the fittings of the $N(h)$ and the $\rho(h)$ of the dendrite with $V=34$ μm/sec. We show the values of α and β for each V in Table I. The profiles exhibit good linearity in the fitted regions. The error of the exponent β is large because of the large variance of the $P(\xi)$.

The height distributions and the number density profiles for four different supersaturations show scale-invariant power laws, and both scaling exponents, α and β, approximately satisfy the relation $\alpha=\beta+1$ (see Table I). These results show fractality of the competitive growth and the structure of the side branches of a dendritic crystal. On the other hand, we obtained $\alpha\approx 1.9$ in the CML model, and $\alpha\approx 1.8$ in our simple needle model of the $(1+1)$-dimensional system [22]. Rossi obtained $\alpha\approx 1.85$ and $\beta\approx 0.83$ in the $(1+1)$-dimensional system [26]. Cates has solved the quasistatic mean-field equations for branchless DLA, and obtained $\beta=1$ [28]. Our experimental results slightly differ from the results of these simulations, because of the following: (i) Each branch in the simulations and theories corresponds to a geometrical line. However, our branches are thick. We conjecture that due to this nonzero width, the length of the longer linear branches might have been affected much more than the length of shorter branches, because longer branches require more solute. Therefore, the value of α might be greater. (ii) Needles or branches in the simulations and theory begin to grow simultaneously from a line seed. However, in our experiments, branches are formed successively from the region near the growing tip. In our system, when a new branch is formed, longer branches are already present nearby. These longer branches affect the growth of the newly formed branches, resulting in more screened shorter branches than in a linear seed system. Therefore, α tends to be larger.

As shown in Figs. 4(b) and 7, the profiles gradually deviate from the power laws at a certain critical height. This indicates a transition of the growth dynamics from competitive scale-invariant growth to independent growth. If the surviving branches begin to grow independently from the other surviving branches, they grow following a new power law [24], and finally acquire a constant velocity whose value is

TABLE I. Summary of exponents α and β for various tip velocities of a stem V.

V (μm/sec)	Region (μm)	α	β
34	$9.5\leqslant h\leqslant 30.3$	2.2 ± 0.1	1.2 ± 0.2
($L=264$ μm)	$9.5\leqslant h\leqslant 49.5$	2.12 ± 0.1	1.1 ± 0.1
34	$66\leqslant h\leqslant 149$	2.1 ± 0.2	1.2 ± 0.4
($L=2635$ μm)	$66\leqslant h\leqslant 247$	2.2 ± 0.1	1.3 ± 0.2
49	$66\leqslant h\leqslant 149$	2.2 ± 0.2	1.2 ± 0.4
	$66\leqslant h\leqslant 247$	2.08 ± 0.09	1.2 ± 0.2
58	$66\leqslant h\leqslant 149$	2.3 ± 0.1	1.2 ± 0.4
	$66\leqslant h\leqslant 198$	2.2 ± 0.1	1.2 ± 0.2
72	$66\leqslant h\leqslant 149$	2.3 ± 0.2	1.2 ± 0.4

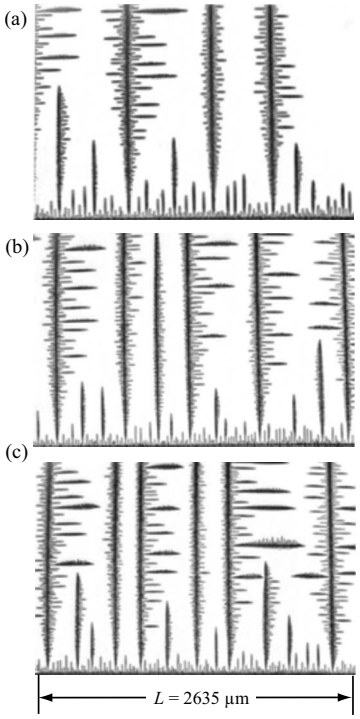

FIG. 5. Three different dendrites at higher supersaturation. The tip velocities are (a) 49 μm/sec, (b) 58 μm/sec, and (c) 72 μm/sec, and $L=2635$ μm.

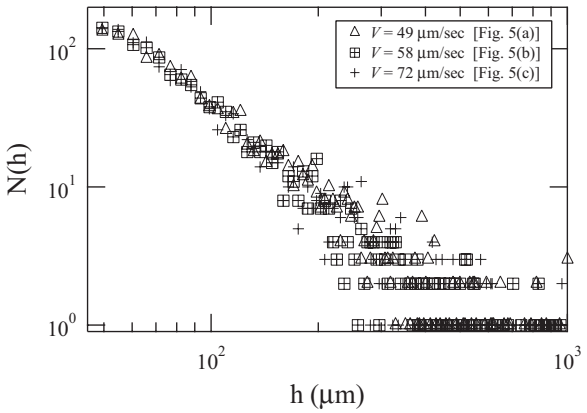

FIG. 6. Height distributions of the branches of dendrites with tip velocities of 49, 58, and 72 μm/sec, and $L=2635$ μm shown in Figs. 5.

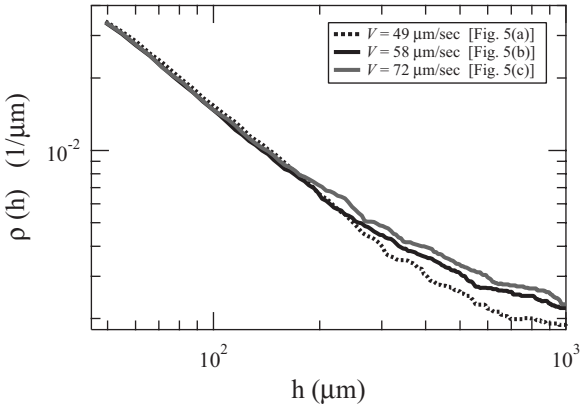

FIG. 7. Number density distributions of branches of the dendrites with tip velocities of 49, 58, and 72 μm/sec, and $L=2635$ μm shown in Figs. 5.

the same as the tip velocity of the stem. As the dendrite grows at higher supersaturation, the critical height decreases, as shown in Fig. 5. To verify the transition more precisely, we will conduct additional experiments, and report the results in a future publication.

IV. CONCLUSION

In summary, we have experimentally investigated the height distributions and number density profiles of side branches of NH_4Cl dendritic crystals for various supersaturated solutions. The distributions and profiles exhibit power laws, and the scaling exponents α and β obey the relation $\alpha=\beta+1$. Furthermore, α and β are independent of the supersaturation levels. These results are consistent with the predictions of numerical simulations and theories of diffusion-limited needle growth.

ACKNOWLEDGMENT

We would like to thank Katsuya Honda for many helpful suggestions and comments.

[1] T. A. Witten and L. M. Sander, Phys. Rev. Lett. **47**, 1400 (1981).
[2] D. G. Grier, D. A. Kessler, and L. M. Sander, Phys. Rev. Lett. **59**, 2315 (1987).
[3] S. C. Huang and M. E. Glicksman, Acta Metall. **29**, 701 (1981).
[4] S. C. Huang and M. E. Glicksman, Acta Metall. **29**, 717 (1981).
[5] Y. Sawada, A. Dougherty, and J. P. Gollub, Phys. Rev. Lett. **56**, 1260 (1986).
[6] W. W. Mullins and R. F. Sekerka, J. Appl. Phys. **35**, 444 (1964).
[7] E. Brener, H. Müller-Krumbhaar, and D. Temkin, Phys. Rev. E **54**, 2714 (1996).
[8] H. Honjo and Y. Sawada, J. Cryst. Growth **58**, 297 (1982).
[9] A. Dougherty, P. D. Kaplan, and J. P. Gollub, Phys. Rev. Lett. **58**, 1652 (1987).
[10] R. Pieters and J. S. Langer, Phys. Rev. Lett. **56**, 1948 (1986).
[11] Q. Li and C. Beckermann, Phys. Rev. E **57**, 3176 (1998).
[12] D. P. Corrigan, M. B. Koss, J. C. LaCombe, K. D. de Jager, L. A. Tennenhouse, and M. E. Glicksman, Phys. Rev. E **60**, 7217 (1999).
[13] O. Wittwer and J. H. Bilgram, Phys. Rev. E **74**, 041604 (2006).
[14] Y. Couder, F. Argoul, A. Arnéodo, J. Maurer, and M. Rabaud, Phys. Rev. A **42**, 3499 (1990).
[15] U. Bisang and J. H. Bilgram, Phys. Rev. E **54**, 5309 (1996).
[16] U. Bisang and J. H. Bilgram, J. Cryst. Growth **166**, 207 (1996).
[17] H. M. Singer and J. H. Bilgram, Physica D **219**, 101 (2006).
[18] A. Dougherty and R. Chen, Phys. Rev. A **46**, R4508 (1992).
[19] A. Dougherty and A. Gunawardana, Phys. Rev. E **50**, 1349 (1994).
[20] E. Hürlimann, R. Trittibach, U. Bisang, and J. H. Bilgram, Phys. Rev. A **46**, 6579 (1992).
[21] R. González-Cinca and L. Ramírez-Piscina, Phys. Rev. E **70**, 051612 (2004).
[22] H. Sakaguchi, K. Kishinawa, K. Katsuki, and H. Honjo, Phys. Rev. E **75**, 021606 (2007).
[23] H. Sakaguchi, J. Phys. Soc. Jpn. **67**, 96 (1998); H. Sakaguchi and M. Ohtaki, Physica A **272**, 300 (1999); H. Sakaguchi, J. Phys. Soc. Jpn. **73**, 1723 (2004).
[24] Y. Couder, J. Maurer, R. González-Cinca, and A. Hernández-Machado, Phys. Rev. E **71**, 031602 (2005).
[25] G. Rossi, Phys. Rev. A **34**, 3543 (1986).
[26] G. Rossi, Phys. Rev. A **35**, 2246 (1987).
[27] P. Meakin, Phys. Rev. A **33**, 1984 (1986).
[28] M. E. Cates, Phys. Rev. A **34**, 5007 (1986); K. Kassner, Phys. Rev. A **42**, 3637 (1990).
[29] D. S. Graff and L. M. Sander, Phys. Rev. E **47**, R2273 (1993); J. Krug, K. Kassner, P. Meakin, and F. Family, Europhys. Lett. **24**, 527 (1993); J. Krug, Adv. Phys. **46**, 139 (1997).
[30] J. P. Wittmer, M. E. Cates, A. Johner, and M. S. Turner, Europhys. Lett. **33**, 397 (1996).
[31] R. Trivedi and K. Somboonsuk, Acta Metall. **33**, 1061 (1985).
[32] H. Honjo and S. Ohta, Phys. Rev. A **45**, R8332 (1992).
[33] A. Tanaka and M. Sano, J. Cryst. Growth **125**, 59 (1992).